

CP violation in the annihilation $e^+ e^- \rightarrow t \bar{t}$ within the Model-III of the two-Higgs-doublet extension

Chao-Hsi Chang^{a,c}, Han Liang^b, Jiang Yi^b, Li Xue-Qian^{a,c,d}
Ma Wen-Gan^{a,b,c}, Zhou Hong^b and Zhou Mian-Lai^b

^aCCAST (World Laboratory), P.O.Box 8730, Beijing 100080, China

^bModern Physics Department, University of Science and
Technology of China, Anhui 230027, China

^cInstitute of Theoretical Physics, Academia Sinica, P.O.Box 2735, Beijing 100080, China.

^dDepartment of Physics, Nankai University, Tianjing 300071, China.

Abstract

The CP-violating effects are studied in the electron-positron annihilation to produce $t\bar{t}$ pair within the Model-III of the two-Higgs-doublet extensions, which allows flavor changing neutral currents via Higgs exchanges. Complete analytical expressions for the form factors of the top quark electric and weak dipole moments induced in the model are presented. Several observables sensitive to the CP violation are calculated. The dependences of the CP-violating effects on Higgs boson masses and the possible phase angles are discussed. We find that the CP-violating observables can be of the order of 10^{-4} in general, but may reach to 10^{-3} for the most favorable parameters.

PACS: 11.30.Er, 12.60.Fr, 14.65.Ha, 13.65.+i

I. Introduction

Symmetries play important role in physics. In the real physical world, some of the symmetries are exact and some are broken. The symmetry CP was found to be broken in neutral kaon system in 1964 by Christenson, Cronin, Fitch and Turlay[2]. Since the discovery on CP violation, more than 30 years have passed. Various models have been proposed to explain the observed CP violation in $K^0 - \bar{K}^0$ mixing. It is well known that the Kobayashi-Maskawa(KM) mechanism in the Standard Model(SM) framework is consistent with all experimental data. Whereas to explain the exist experimental data, there is still some room for certain extensions of the SM. Especially, it seems that to solve the so-called baryon genesis problem of the universe, the strength of the CP violation due to the KM mechanism is not strong enough and it indicates some new source(s) of CP violation else is required. Therefore the problem on the source(s) of CP violation should be considered being still open. In the literatures[3, 4], it is pointed out that the extended Higgs sector in the two-Higgs-doublet model(THDM) may open many different and interesting CP violating sources. Indeed, if CP violation is really related to the Higgs sector of a SM extension, such as in the THDM-III which we are considering in this work, the verification on the CP violation source is crucial not only for the problem itself, but also for understanding the electroweak symmetry breaking. Moreover as mentioned above, it also must be interesting for cosmology study, i.e., opening some solutions to the baryon-genesis problem in the universe.

In the commonly discussed THDM, the natural flavor conservation(NFC) condition is invoked to assure the absence of flavor changing scalar interactions(FCSI) by certain symmetry. Then the THDM with the NFC condition is subdivided into two modes, namely Model-I and Model-II. In Model-I, both the up and down type quarks achieve their masses from the same Higgs doublet, and in Model-II the quarks do so from different doublets. In fact, to compare with experimental data, it is not so necessary to put a symmetry to dictate the NFC condition, whereas, there is another possible mode of the THDM, which is popularly called as Model-III now. In this model instead of placing the NFC constraints by a discrete symmetry, the Yukawa couplings for FCSI are introduced as usual done, i.e., in the meantime, they also generate the fermions' masses with the nonzero vacuum expectation value of the Higgs. The consequence of the way to introduce the Yukawa couplings for the THDM-III, is that the coupling will be proportional to the masses of the

coupled fermions. Considering the fact that the most fundamental fermions in the SM except top-quark have a small mass, the FCSI in the THDM-III at the tree level would not exist substantially at low mass scales. As we know that two years ago the CDF and D0 collaborations found the top quark has a so large mass(i.e., now the world average value: $m_t = 175.6 \pm 5.5 \text{ GeV}$)[1]. Therefore it is believed that careful study on the processes relevant to the top quark would be the most possible approach to new physics. As the heavy top quark will strongly suppress the effects of its mixing with other generations in the SM, the GIM mechanism of unitary constraints leads to very small CP-violation effects, although it makes the greater CP effects due to KM mechanism in B meson decays and the B meson systems than those in K systems. Hence any observation of the CP violation in top quark production and decays would give interesting informations, because it may relate to the physics beyond the SM including the THDM-III. In addition, the lifetime of top quark is so short that there is no enough time to make hadrons before its weak decay, the ‘phase information’ of the produced top quark, which contains the CP signature, will be kept in its decay products very well without ‘disturbing’ by hadronization. Therefore to observe the CP violation in top quark production makes sense and becomes accessible.

Previously, motivating CP violation in the top production has been extensively investigated[5][6][7]. In most of these works, the effects from the electric and weak dipoles and the CP-violating observables in the process $e^+e^- \rightarrow t\bar{t}$ are investigated in a model-independent way. Some works are contributed to the CP-violating effects induced by the Higgs sector in the THDM without FCSI’s and the MSSM in the process.

In this paper we concentrate on the CP violation effects in the process of the top quark pair production at e^+e^- colliders, which are originated from the THDM-III. We organize the paper as follows: In section 2, we will briefly outline the THDM-III for self containment and give the relevant vertices of Yukawa couplings involving CP-violating phases. In section 3, the complete electric and weak dipole moment form factors of the top quark within the THDM-III are calculated. In section 4, some CP violating sensitive observables for the process $e^+e^- \rightarrow t\bar{t}$ are evaluated and discussed. Finally a short summary is given.

2. The third type of the two Higgs doublet model(THDM-III)

Generally in the third type of the two-Higgs-doublet model, the up-type and down-type quarks couple simultaneously to more than one scalar doublet. We consider the THDM-III has two scalar $SU(2)_w$ doublets, ϕ_1 and ϕ_2 :

$$\phi_1 = \begin{pmatrix} \phi_1^+ \\ \phi_1^0 \end{pmatrix}, \quad \phi_2 = \begin{pmatrix} \phi_2^+ \\ \phi_2^0 \end{pmatrix}, \quad (2.1)$$

with Lagrangian

$$\mathcal{L}_\phi = D^\mu \phi_1^\dagger D_\mu \phi_1 + D^\mu \phi_2^\dagger D_\mu \phi_2 - V(\phi_1, \phi_2), \quad (2.2)$$

where $V(\phi_1, \phi_2)$ is the general potential which is consistent with the gauge symmetries. Since there is no global symmetry that distinguishes the two doublets in the THDM-III, without loss of generality we assume $v_2 = 0$, $\beta = \pi$ with $\tan \beta \equiv v_2/v_1$. Then we have

$$\langle \phi_1 \rangle = \begin{pmatrix} 0 \\ v/\sqrt{2} \end{pmatrix}, \quad \langle \phi_2 \rangle = 0 \quad (2.3)$$

where $v \simeq 246 \text{ GeV}$. Three of the components of ϕ_1 become the longitudinal components of the W^\pm and Z^0 bosons, and the physical spectrum contains also the charged scalar bosons H^\pm , the neutral scalars h^0 and H^0 and the pseudoscalar A^0 .

$$\begin{aligned} H^0 &= \sqrt{2}[(Re\phi_1^0 - v) \cos \alpha + Re\phi_2^0 \sin \alpha], \\ h^0 &= \sqrt{2}[-(Re\phi_1^0 - v) \sin \alpha + Re\phi_2^0 \cos \alpha], \\ A^0 &= \sqrt{2}(-Im\phi_2^0), \\ H^\pm &= -\phi_2^\pm. \end{aligned} \quad (2.4)$$

where α is the mixing angle of the CP-even neutral Higgs bosons. The physical charged Higgs state is orthogonal to G^\pm . Then the charged Goldstone bosons G^\pm are

$$G^\pm = -\phi_1^\pm. \quad (2.5)$$

In this model there are still six free parameters which include the masses of the five neutral and charged Higgs bosons(m_{h^0} , m_{H^0} , m_{A^0} , m_{H^\pm}) and the mixing angle α . The Yukawa couplings to quarks are[8],

$$\mathcal{L}_Y^Q = \lambda_{ij}^U \bar{Q}_i \tilde{\phi}_1 U_j + \lambda_{ij}^D \bar{Q}_i \phi_1 D_j + \xi_{ij}^U \bar{Q}_i \tilde{\phi}_2 U_j + \xi_{ij}^D \bar{Q}_i \phi_2 D_j + h.c.. \quad (2.6)$$

In above equation we define $\tilde{\phi}_{1,2} = i\tau_2\phi_{1,2}^*$, U_i and D_i are the SU(2) doublets of left-handed quark states and Q_i ($i = 1, 2, 3$) are the SU(2) singlets of right-handed quark states. In the first two terms in Eq.(2.6) involving the ϕ_1 doublet generate the quark masses, while ϕ_2 appearing in the following two terms is responsible for the new interactions. With the usual manipulations λ^U and λ^D can be expressed in terms of the mass matrices $\frac{\sqrt{2}M^U}{v}$ and $\frac{\sqrt{2}M^D V_{KM}^\dagger}{v}$, where V_{KM} is the Kobayashi-Maskawa(KM) matrix. ξ_{ij}^U and ξ_{ij}^D are the 3×3 matrices which determine the strengths of the flavor changing neutral scalar vertices. The ξ s are all free parameters and can only be constrained by the observation of experiments relating to FCSI. The CP violation can be induced in this model by having complex ξ s and the phase angle in KM matrix. In order to apply the THDM-III to our specific process, we have to employ some definite ansatz on the ξ_{ij}^U and ξ_{ij}^D . Here we use the Cheng-Sher Ansatz (CSA)[9] and the Yukawa couplings can be parametrized as

$$|\xi_{ij}^{U,D}| = g \frac{\sqrt{m_i m_j}}{m_W} |\lambda_{ij}^{U,D}|. \quad (2.7)$$

In principle the parameters $\lambda_{ij}^{U,D}$ need to be constrained by available phenomenology. Due to the fact that the factor $\frac{\sqrt{m_i m_j}}{m_W}$ for light quarks is quite small, the observations of the FCSI of the THDM-III for light quarks are quite difficult, so far the substantial constraints are lack i.e., the $\lambda_{ij}^{U,D}$ mixing parameters are not well constrained. In order to simplified our analysis and have a possible and definite CP violation effect, we will take $|\lambda_{ij}^{U,D}| = \frac{1}{\sqrt{2}}$, which may make a comparison of $\lambda_{ij}^{U,D}$ to the usual gauge couplings of $SU(2) \times U(1)$ in the SM. Whereas in general $\lambda_{ij}^{U,D}$ could be complex so as to induce an additional CP violation source. Thus we write $\lambda_{ij}^{U,D}$ as

$$\lambda_{ij}^{U,D} = \frac{1}{\sqrt{2}} e^{\theta_{ij}^{U,D}}. \quad (2.8)$$

where $\theta_{ij}^{U,D}$ ($i, j = 1, 2, 3$) are the phase angles of the complex parameters $\lambda_{ij}^{U,D}$. We denote $\theta_{33}^U = \theta_1$ and $\theta_{33}^D = \theta_2$, and try to concern the CP violation caused by them in our calculation.

3. CP-violating dipole couplings of top quark

In the process $e^+e^- \rightarrow t\bar{t}$ the CP-violating effects come from the electric and weak dipole moments of top quark. In this section we analyze the

THDM-III contributions to electric and weak dipoles of the top quark. In the THDM-III, additional complex couplings can be introduced and lead to CP violation in top quark physics. Generally it is assumed that the couplings $-ie\Gamma_\mu^{\gamma,Z}$, which are the interactions between the top quark and γ , Z^0 . The couplings include CP violation phases and have the form factors as:

$$\Gamma_\mu^j = V^j \gamma_\mu + A^j \gamma_\mu \gamma_5 + \frac{d_j}{2m_t} i \gamma_5 (p_t - p_{\bar{t}})_\mu, \quad (j = \gamma, Z), \quad (3.1)$$

with

$$V^\gamma = \frac{2}{3}, \quad A^\gamma = 0, \quad V^Z = \frac{1}{4 \sin \theta_W \cos \theta_W} (1 - \frac{8}{3} \sin^2 \theta_W), \quad A^Z = -\frac{1}{4 \sin \theta_W \cos \theta_W}. \quad (3.2)$$

In Eq.(3.1), the d_γ and d_Z are called the electric and weak dipole moment form factors, respectively. In figure (1) we represent the one-loop Feynman diagrams of the vertices which contribute to the electric and weak dipole form factors of the top quark. In our consideration we ignore the couplings of the quarks in the first and second generations to Higgs and Goldstone bosons, because of their very light masses. One can expect that if the Higgs boson masses are not much heavier than the top quark, there would be a large values for electric and weak dipoles induced by the THDM-III one-loop corrections. The relevant Feynman rules of the interactions with complex couplings are given in figure (2). The explicit expressions of the electric and weak dipole form factors of top quark in the framework of the THDM-III are listed in Appendix.

The size of the dipole moment form factors d_γ and d_Z depends strongly on the phases of the parameters ξ s in the THDM-III. The electric dipole observations on neutron and other experiments should put constraints on the phases of ξ s. In the calculation on the neutron dipole it is known that there are some theoretical uncertainties for the neutron struction of quarks, thus at present calculation we put the experimental constraint from neutron dipole aside and make more general analysis for the CP-violation effects in top quark production. In the numerical evolution we take the input parameters as $m_b = 4.5$ GeV, $m_Z = 91.187$ GeV, $m_W = 80.33$ GeV, $m_t = 175$ GeV, $G_F = 1.166392 \times 10^{-5} (GeV)^{-2}$ and $\alpha(0) = \frac{1}{137.036}$ [11], here we ignore the running of α which can only give rise to minor changes to our results. The real and imaginary parts of the d_γ and d_Z as the functions of the energy

of the center mass system (CMS) of the incoming electron and positron, are plotted in Fig.3(1). There we take the mass values of Higgs bosons as $m_{h^0} = 100 \text{ GeV}$, $m_{H^0} = 200 \text{ GeV}$, $m_{H^\pm} = 150 \text{ GeV}$ and $m_A = 250 \text{ GeV}$, the mixing angle of the neutral Higgs bosons as $\alpha = \frac{\pi}{6}$, the CP-violating phase angles as $\theta_1 = \frac{\pi}{4}$ and $\theta_2 = \frac{\pi}{2}$. The absolute values of both the real and imaginary parts of the dipoles are enhanced at vicinity of the energy region of the top pair production threshold and tend to vanish when the center-of-mass energy \sqrt{s} is getting larger. In Fig.3(2), Fig.3(3) and Fig.3(4), the values of electric and weak dipoles as the functions of the masses of the Higgs bosons m_{h^0} , m_{H^\pm} and m_A are depicted, respectively, with $\sqrt{s} = 500 \text{ GeV}$ and the other parameters being the same as those in Fig.3(1). The dependences of the quantities of the dipoles on the masses of h^0 and A^0 Higgs bosons are clear, but the dipoles do not depend on the mass of H^\pm very much. In Fig.3(2) the curves for the real and imaginary parts of weak dipole are raised quantitatively at the position of $m_h \sim 400 \text{ GeV}$. That is because of the resonance effects contributed by the diagrams Fig.1(6,7,8,9) with the condition $\sqrt{s} = m_h + m_Z$ being satisfied. There is a small spike on each of the four curves in Fig.3(3) at the position of $m_{H^\pm} = m_t + m_b \sim 180 \text{ GeV}$ due to the resonance effect coming from the one-loop diagrams in Fig.1(5). The dependences of the dipoles on the mass of H^0 are not shown in figure, since the features of these dependences are similar with that in Fig.3(2) due to the similar Yukawa couplings with quarks. The electric and weak dipoles as the functions of the CP-violating phase angles $\theta_1(\theta_{33}^U)$ and $\theta_2(\theta_{33}^D)$ are shown in Fig.3(5) and Fig.3(6), respectively. In each of these two figures we take the input parameter values as before and assume the phase angles θ_2 and θ_1 to be zero in Fig.3(5) and Fig.3(6), respectively. We can see that the dipoles mainly come from the phase angle θ_1 and take maximal absolute values when θ_1 has the values around 125° and 235° . The contributions to dipoles from the phase angle θ_2 are two order smaller than from the phase angle θ_1 . That can be understood because the CP effect from the complex phase angle θ_1 is in proportion to top quark mass, whereas the effect from the phase angle θ_2 is in proportion to bottom quark mass, which can be read from the coupling Feynman rules shown in Fig.2.

4. CP violating observables in the process $e^+e^- \rightarrow t\bar{t}$

At the future electron-positron collider CP violation in the $t\bar{t}$ pair production can be searched by various means[5][7]. In this section, we present

some CP violation observables precisely and then discuss the behaviors of CP violation effects due to the electric and weak dipoles. The presence of electroweak dipole of the top quark will induce the CP violation in the process $e^+e^- \rightarrow t\bar{t}$. It leads asymmetry in the polarizations of the top quark and top anti-quark. These polarizations can be determined by analyzing the energy and angular distributions of the charged lepton(antilepton) particles produced by the top quark(top anti-quark) sequential leptonic decay. The analytic expressions for these distributions and the CP-violating angular asymmetries ($A_{ch}(\theta_0)$, $A_{FB}(\theta_0)$) have been obtained by Poulou and Rindani[10]. In those expressions the CP-violating effects in the consequent decays of top quark and top antiquark are ignored. The total lepton charge asymmetry with a angle cutoff θ_0 of the charged lepton is defined as:

$$A_{ch}(\theta_0) = \frac{\int_{\theta_0}^{\pi-\theta_0} d\theta_l \left(\frac{d\sigma^+}{d\theta_l} - \frac{d\sigma^-}{d\theta_l} \right)}{\int_{\theta_0}^{\pi-\theta_0} d\theta_l \left(\frac{d\sigma^+}{d\theta_l} + \frac{d\sigma^-}{d\theta_l} \right)}. \quad (4.1)$$

The charged leptonic forward-backward asymmetry with a charged lepton angle cutoff θ_0 is defined in the form as:

$$A_{FB}(\theta_0) = \frac{\int_{\theta_0}^{\frac{\pi}{2}} d\theta_l \left(\frac{d\sigma^+}{d\theta_l} - \frac{d\sigma^-}{d\theta_l} \right) - \int_{\frac{\pi}{2}}^{\pi-\theta_0} d\theta_l \left(\frac{d\sigma^+}{d\theta_l} - \frac{d\sigma^-}{d\theta_l} \right)}{\int_{\theta_0}^{\pi-\theta_0} d\theta_l \left(\frac{d\sigma^+}{d\theta_l} + \frac{d\sigma^-}{d\theta_l} \right)}. \quad (4.2)$$

These two types of angular asymmetries can be the measures of CP violation in the process $e^+e^- \rightarrow t\bar{t}$ in unpolarized case. The relevant expressions of A_{ch} and A_{FB} for this process can be found in Ref.[10].

We use the input parameters as described in the above section and take a leptonic angle-cutoff $\theta_0 = 30^\circ$ in numerical calculations. The charged leptonic charge asymmetry A_{ch} and the forward-backward asymmetry A_{FB} versus the center-of-mass energy of e^+e^- system are depicted in Fig.4(1). In this figure, the absolute value of the asymmetry A_{ch} , in general, is smaller than that of A_{FB} when the same parameters have been taken. Actually, if the charged leptonic angle-cutoff θ_0 is changed smaller, the value of the asymmetry A_{ch} will decrease greatly, e.g. when the cutoff is changed into 9° , the asymmetry A_{ch} will decrease by an order of magnitude comparing with that for the former choice. From this figure we can see that the CP violation asymmetries have threshold effects in the energy region near $2 m_t$ clearly. Due to the phase space effects, there is a small spike on each of the

curves in Fig.4(1). Our numerical calculation shows that when the leptonic cutoff-angle is changed to a smaller value from 30° , the spikes are shifted to the left side until it vanishes. The dependences of the two types of the CP-violation asymmetries on the masses of Higgs bosons h^0 , H^\pm and A^0 are plotted in Fig.4(2) and Fig.4(3), respectively. The asymmetries depend on the masses of the CP-odd neutral Higgs boson and the CP-even neutral Higgs boson A^0 and m_{h^0} precisely, but they are not sensitive to the mass of charged Higgs boson H^\pm . Again, in Figs.4(2,3) we can see the effects on the curves due to the resonances at the positions of m_{H^\pm} and m_{h^0} as well as $m_{H^\pm} \sim m_t + m_b \sim 180$ GeV and $m_{h^0} \sim 400$ GeV respectively. The two asymmetries attributed to the electric and weak dipoles versus the CP-violation phase angles $\theta_1(\theta_{33}^U)$ and $\theta_2(\theta_{33}^D)$ are plotted in Fig.4(4) and Fig.4(5), respectively. In each of these two figures, the calculated results are obtained in each case by assuming one of the phase angles being zero and with the same input parameters as those being taken before. They show again that the CP-violation effects mainly come from the phase angle θ_1 and have maximal absolute values when θ_1 has the values about 125° or 235° . The quantitative contributions to the asymmetries due to the CP-violating phase angle θ_2 are smaller than those due to the phase angle θ_1 .

There are alternative choices for the CP-odd observables to observe CP violation, of which some can be better, but some not. Moreover, to distinguish different CP violation sources, various CP-odd observables are needed in general. For the purpose and to try one more observable, let us introduce a new CP asymmetric parameter by means of the vectors \vec{s} and $\vec{\omega}$, i.e., the spin and the polarization vectors of the top quark respectively. The two vectors are three dimensional essentially. The vector \vec{s} is normalized by definition, and the vector $\vec{\omega}_t$ is defined as[12]

$$\omega_{t,i} = \frac{N_t(\vec{s} = \hat{e}_i) - N_t(\vec{s} = -\hat{e}_i)}{N_t(\vec{s} = \hat{e}_i) + N_t(\vec{s} = -\hat{e}_i)}. \quad (4.3)$$

where $N_t(\vec{s} = \hat{e}_i)$ means the event number of the top quark with a spin vector as $\vec{s} = \hat{e}_i$. Here \hat{e}_i ($i=1, 2, 3$) are the normalized basis vectors of a Cartesian coordinate frame. Note that in the rest frame of the top quark, the four-dimensional spin vector s_μ of the top quark becomes $(0, \vec{s})$. To calculate the polarization vector $\omega_{t,i}$ in the CMS of electron and positron, we shall introduce the coordinate system (x', y', z') , where z' -axis is along the outgoing direction of top quark and y' -axis is perpendicular to the production

plane of top quark pair. The commonly used coordinate system (x, y, z) in the CMS of initial states, is defined as: z-axis is along the incoming direction of e^- and y-axis is perpendicular to the production plane of top pair. The angle between the axes z and z' is just the angle θ between the incoming electron and the outgoing top quark. Since we do not observe both polarizations of top and anti-top quarks in the meantime, thus to focus the polarization of the top quark, we sum up the spin of anti-top quark when calculating polarization vector $\vec{\omega}_t$. In this way, for the top quark spin $\vec{s} = \hat{e}_{z'}$, the corresponding four-dimension spin vector in (x', y', z') system becomes as[12]

$$(s)_\mu = (\beta\gamma, 0, 0, \gamma), \quad (4.4)$$

where $\gamma = \frac{\sqrt{s}}{2m_t}$ and $\beta = \sqrt{1 - \gamma^{-2}}$. For the top quark spin vectors $\vec{s} = \hat{e}_{x'}, \hat{e}_{y'}$, the corresponding four-dimension spin vectors are

$$(s)_\mu = (0, 1, 0, 0) \quad and \quad (s)_\mu = (0, 0, 1, 0), \quad (4.5)$$

respectively.

Analogously, the vectors $\vec{\omega}_{\bar{t}}$ for the top anti-quark can be defined too. Now let us introduce the so-called spin-momentum correlation-parameter for the top quark outgoing in a specific direction,

$$\xi_{CP} = (\hat{p}_{e^-} \times \hat{p}_t) \cdot (\vec{\omega}_t - \vec{\omega}_{\bar{t}}), \quad (4.6)$$

and it is easy to see that the correlation parameter is CP-odd. Here \hat{p}_{e^-} and \hat{p}_t are unit vectors of the three-dimensional momenta of the electron and the top quark, and $\vec{\omega}_t$ and $\vec{\omega}_{\bar{t}}$ are the polarization vectors of the top quark and the top anti-quark in the (x, y, z) system. We know that if CP conservation is hold, the polarization vectors $\vec{\omega}_t$ and $\vec{\omega}_{\bar{t}}$ of the top quark and the top anti-quark cannot have nonzero components perpendicular to the production plane *i.e.*, $\omega_{t,y} = \omega_{\bar{t},y} = 0$, and consequently the parameter ξ_{CP} must be zero. If CP violates in the process, only the components of the polarization vectors $\vec{\omega}_t$ and $\vec{\omega}_{\bar{t}}$ perpendicular to the production plane(ω_y) contribute to the asymmetry parameter ξ_{CP} . Thus to calculate the asymmetry observable ξ_{CP} , we have to compute the polarization vectors of the top quark and the top anti-quark in y-component only. Namely the observable ξ_{CP} can be measured by the possible asymmetry in the polarization vectors of t and \bar{t} perpendicular to the production plane.

Taking a cutoff for the top quark angle $\theta_{cut} = 9^\circ$, we compute the spin-momentum correlation parameter ξ_{CP} numerically by the above definitions and plot its average value $\langle \xi_{CP} \rangle$ as a function of \sqrt{s} in Fig.5(1). The threshold influence at the energy region near $\sqrt{s} \sim 2 m_t$ and smooth variation (approaches to 4×10^{-4} with the increasing of \sqrt{s}) of the average value of the asymmetry parameter $\langle \xi_{CP} \rangle$, are shown clearly in the figure. The dependences of the average value of the CP-violation parameter, $\langle \xi_{CP} \rangle$, on the masses of Higgs bosons are represented in Fig.5(2). There are similar dependences on the Higgs boson masses as those illustrated in the previous cases for the electric and weak dipoles of the top quark and the other observables. We can also see that the resonance effects are manifested on the curves for the dependences on the masses m_{h^0} and m_{H^\pm} , e.g. when $m_{h^0} = 400 \text{ GeV}$ and $m_{H^\pm} = m_t + m_b$, respectively. The parameter $\langle \xi_{CP} \rangle$ versus CP-violation angles θ_1 and θ_2 are depicted in Fig.5(3) respectively, by assuming the CP-violation angles θ_2 and θ_1 to be zero in turn. Thus it is seen clearly that the CP-violation here takes source mainly from the phase angle θ_1 and has the maximal absolute value when θ_1 has the values about 125° and 235° , whereas the contribution to the asymmetry parameter due to the CP-violating phase angle θ_2 is much smaller than that due to the phase angle θ_1 .

5. Summary

We have calculated the contributions to the electric and weak dipoles of the top quark in the frame of the THDM-III by introducing complex phase parameters ξ^U and ξ^D . The complete analytical expressions of the dipole form factors of top quark are presented. Some observables which are sensitive to CP violation are discussed. The form factors for the electric and weak dipoles, the CP-violating observables A_{ch} , A_{FB} and $\langle \xi_{CP} \rangle$ all depend on the masses of Higgs bosons, the CP-violating phase angles θ_1 and θ_2 and the CMS energy in electron-positron system as well.

We have found that the electric and weak dipole form factors and other observables are enhanced in the threshold region of top pair production. The CP-violation asymmetries are mostly related to the neutral Higgs bosons A^0 and h^0 masses and the phase angle θ_1 . The numerical results show that they are in general of order of 10^{-4} , and the electric, weak dipoles and the spin-momentum asymmetry $\langle \xi_{CP} \rangle$ can reach about 10^{-3} quantitatively. In the sense, being a directly measurable observable, $\langle \xi_{CP} \rangle$ may be a better one

than the others.

In summary, the values for the CP-odd observables considered in the paper may fall into the ability for the underconsidering colliders such as NLC, which can reach to a high enough energy and luminosity i.e., the asymmetries may become measurable for the powerful colliders. Therefore we would like to conclude that the top quark pair production at a very high energy e^+e^- collider may serve as a process for probing and hopefully investigating the CP violation sources in the THDM-III by measuring various CP-odd observables.

Acknowledgement: These work was supported in part by the National Natural Science Foundation of China (project numbers: 19675033 and 19677102) and the Grant of Chinese Academy of Science. The authors would like to thank Dr. J. P. Ma for useful comments.

Appendix

The electric dipole form factor d_γ , taking the source of the THDM-III, can be presented explicitly as:

$$\begin{aligned}
d_\gamma = & \frac{im_t^2 g^2}{96m_W^2 \pi^2} (3(e^{(i\theta^D+i\theta^U)} - e^{(-i\theta^D-i\theta^U)})m_b^2 C_0^1 \\
& + (e^{(2i\theta^U)} - e^{(-2i\theta^U)})m_t^2 C_{11}^2 - (e^{(i\theta^D+i\theta^U)} - e^{(-i\theta^D-i\theta^U)})m_b^2 C_{11}^3 \\
& + (m_t^2 - m_b^2)C_{11}^3 - (e^{(2i\theta^U)} - e^{(-2i\theta^U)})m_t^2 \cos^2 \alpha C_{11}^4 \\
& - 3(m_t^2 - m_b^2)C_{11}^1 + 3(e^{(i\theta^D+i\theta^U)} - e^{(-i\theta^D-i\theta^U)})m_b^2 C_{11}^1 \\
& - 2(m_t^2 - m_b^2)C_{12}^3 + 6(m_t^2 - m_b^2)C_{12}^1 \\
& + (m_t^2 - m_b^2)C_{21}^3 - 3(m_t^2 - m_b^2)C_{21}^1 \\
& - 2(m_t^2 - m_b^2)C_{23}^3 + 6(m_t^2 - m_b^2)C_{23}^1 \\
& - 2(e^{(i\theta^U)} - e^{(-i\theta^U)})m_t^2 \cos \alpha C_{11}^4 \sin \alpha \\
& + 2(e^{(i\theta^U)} - e^{(-i\theta^U)})m_t^2 \cos \alpha C_{11}^5 \sin \alpha \\
& - (e^{(2i\theta^U)} - e^{(-2i\theta^U)})m_t^2 C_{11}^5 \sin^2 \alpha) \quad (A.1)
\end{aligned}$$

The weak dipole form factor d_Z due to the THDM-III can be presented

explicitly as follows:

$$\begin{aligned}
d_z = & \frac{im_t^2 g^2}{(384m_W^2 \pi^2) \sin \theta_w \cos \theta_w} (6(e^{(i\theta^D+i\theta^U)} - e^{(-i\theta^D-i\theta^U)})m_b^2 \cos 2\theta_w C_0^1 \\
& + 3(e^{(2i\theta^U)} - 1)m_t^2 C_{11}^2 + 6(m_t^2 - e^{(i\theta^D+i\theta^U)}m_b^2)C_{11}^3 \\
& - 3(e^{(2i\theta^U)} + 1)m_t^2 \cos^2 \alpha C_{11}^4 \\
& - 6m_t^2 \cos^2 \alpha C_{11}^5 + 6(e^{(i\theta^D+i\theta^U)} - e^{(-i\theta^D-i\theta^U)})m_b^2 \cos 2\theta_w C_{11}^1 \\
& - 6(m_t^2 - m_b^2) \cos 2\theta_w C_{11}^1 + 3(2 - e^{(-2i\theta^U)} - e^{(2i\theta^U)})m_t^2 C_{12}^2 \\
& + 6(e^{(-i\theta^D-i\theta^U)} + e^{(i\theta^D+i\theta^U)})m_b^2 C_{12}^3 - 12m_t^2 C_{12}^3 \\
& + 3(2 + e^{(-2i\theta^U)} + e^{(2i\theta^U)})m_t^2 \cos^2 \alpha C_{12}^4 + 12m_t^2 \cos^2 \alpha C_{12}^5 \\
& + 12(m_t^2 - m_b^2) \cos 2\theta_w C_{12}^1 - 3m_t^2(C_{21}^2 - 2C_{21}^3) - 3m_t^2 \cos^2 \alpha (C_{21}^4 + C_{21}^5) \\
& - 6(m_t^2 - m_b^2) \cos 2\theta_w C_{21}^1 + 6m_t^2(C_{23}^2 - 2C_{23}^3) + 6m_t^2 \cos^2 \alpha (C_{23}^4 + C_{23}^5) \\
& + 12(m_t^2 - m_b^2) \cos 2\theta_w C_{23}^1 - 3(e^{(-i\theta^U)} + 3e^{(i\theta^U)})m_t^2 \cos \alpha C_{11}^4 \sin \alpha \\
& + 3(e^{(-i\theta^U)} + 3e^{(i\theta^U)})m_t^2 \cos \alpha C_{11}^5 \sin \alpha \\
& + 3(e^{(-i\theta^U)} + e^{(i\theta^U)})m_t^2 \cos \alpha (4C_{12}^4 - 4C_{12}^5 - C_{21}^4 + C_{21}^5 + 2C_{23}^4 - 2C_{23}^5) \sin \alpha \\
& + 3m_t^2(-2C_{11}^4 - (1 + e^{(2i\theta^U)})C_{11}^5 + 4C_{12}^4 + (2 + e^{(-2i\theta^U)} + e^{(2i\theta^U)})C_{12}^5 - C_{21}^4 \\
& - C_{21}^5 + 2C_{23}^4 + 2C_{23}^5) \sin^2 \alpha + 4(e^{(-2i\theta^U)} - e^{(2i\theta^U)})m_t^2 C_{11}^2 \sin^2 \theta_w \\
& + 4(e^{(i\theta^D+i\theta^U)} - e^{(-i\theta^D-i\theta^U)})m_b^2 C_{11}^3 \sin^2 \theta_w \\
& - 4(m_t^2 - m_b^2)C_{11}^3 \sin^2 \theta_w + 4(e^{(2i\theta^U)} - e^{(-2i\theta^U)})m_t^2 \cos^2 \alpha C_{11}^4 \sin^2 \theta_w \\
& + 4(m_t^2 - m_b^2)(2C_{12}^3 - C_{21}^3 + 2C_{23}^3) \sin^2 \theta_w \\
& + 8(e^{(i\theta^U)} - e^{(-i\theta^U)})m_t^2 \cos \alpha (C_{11}^4 - C_{11}^5) \sin \alpha \sin^2 \theta_w \\
& + 4(e^{(2i\theta^U)} - e^{(-2i\theta^U)})m_t^2 C_{11}^5 \sin^2 \alpha \sin^2 \theta_w \\
& + 2(C_{11}^6 - C_{12}^6 - C_{12}^7)(e^{-i\theta^U} - e^{i\theta^U})m_Z^2 (4 \cos 2\theta_W - 1) \sin 2\alpha
\end{aligned} \tag{A.2}$$

Here the following notations are adopted:

$$\begin{aligned}
C_{i,ij}^1 &= C_{i,ij}[p_2, -p_1 - p_2, m_b, m_{H^\pm}, m_{H^\pm}] \\
C_{i,ij}^2 &= C_{i,ij}[p_1, -p_1 - p_2, m_{A^0}, m_t, m_t] \\
C_{i,ij}^3 &= C_{i,ij}[p_1, -p_1 - p_2, m_{H^\pm}, m_b, m_b] \\
C_{i,ij}^4 &= C_{i,ij}[p_1, -p_1 - p_2, m_{h^0}, m_t, m_t] \\
C_{i,ij}^5 &= C_{i,ij}[p_1, -p_1 - p_2, m_{H^0}, m_t, m_t] \\
C_{i,ij}^6 &= C_{i,ij}[-p_1, p_1 + p_2, m_t, m_Z, m_H] \\
C_{i,ij}^7 &= C_{i,ij}[-p_1, p_1 + p_2, m_t, m_h, m_Z]
\end{aligned} \tag{A.3}$$

In above expressions we adopted the definition of the three-point integral functions in Ref.[13] and the references therein.

References

- [1] CDF Collaboration, F. Abe et al., Phys. Rev. Lett. **74**, 2626(1995); D0 Collaboration, S. Abachi et al., *ibid.* **74**, 2632(1995); P.C. Bhat, for the D0 collaboration, talk presented at the Wine and Cheese Seminar at Fermilab, February 1997.
- [2] J.H. Christenson, J.W. Cronin, V.L. Fitch and R. Turlay Phys. Rev. Lett. **13**, 138(1964).
- [3] T.D. Lee, Phys. Rev. **D8**, 1226(1973); S. Weinberg, Phys. Rev. **D42**, 860(1990).
- [4] L. Wolfenstein and Y.-L. Wu, Phys. Rev. Lett. **73**, 2809(1994).
- [5] W. Bernruther, O. Nachtmann, P. Overmann and T. Schroder, Nucl. Phys. **B388**, 53(1992); W. Bernruther and O. Overmann, Z. Phys. **C61**, 599(1994); W. Bernruther and O. Nachtmann, Phys. Lett. **B268**, 424(1991); W. Bernruther and A. Brandenburg, Phys. Lett. **B314**, 104(1993); Phys. Rev. bf D49, 4481(1994); A. Brandenburg, J.P. Ma, R. Munch and O. Nachtmann, Z. Phys. bf C51, 225(1991).
- [6] E. Christova and M. Brandenburg, Phys. Lett. **B315**, 338(1993); E. Christova and M. Fabbrichesi, Phys. Lett. **B315**, 113(1993); D. Atwood and A. Soni, Phys. Rev. **D45**, 2405(1992); A. Bartl, E. Christova and W. Majerotto, Nucl. Phys. **B 460**, 235(1996).
- [7] C.R. Schmidt and M.E. Peskin, Phys. Rev. Lett. **69**, 410(1992); B. Grzadkowski and J. Gunion, Phys. Lett. **B287**, 237(1992); C.R. Schmidt, Phys. Lett. **B293**, 111(1992); E. Christova and M. Fabbrichesi, Phys. Lett. **B320**, 299(1994); B. Grzadkowski W. Keung, Phys. Lett. **B319**, 526(1993); B. Grzadkowski, Phys. Lett. **B305**, 384(1993); B. Grzadkowski, Phys. Lett. **B316**, 137(1993). A. Bartl, et. al, ‘Electroweak dipole moment form factors of the top quark in supersymmetry’, hep-9709219.
- [8] M. Luke and M.J. Savage, Phys. Lett. **B307**, 387(1993).
- [9] T. P. Cheng and M. Sher, Phys. Rev. **D35**, 3484(1987); M. Sher and Y. Yuan, *ibid.* **44**, 1461(1991).

- [10] P. Poulose and S.D. Rindani, Phys. Rev. **D54**, 4326(1996).
- [11] Particle Data Group, R.M. Barnett, et al, Phys. Rev. **D54**, 1(1996).
- [12] Y.S. Tsai, Phys. Rev. **D51**, 3172(1995).
- [13] Kniehl B. A., Phys. Rep. 240(1994)211 and references therein.

Figure captions

Fig.1 The Feynman diagrams which contribute to electric and weak dipoles of top quark.

Fig.2 The Feynman rules of the relevant vertices involving complex coupling constants.

Fig.3(1) The electric and weak dipoles d_γ and d_Z as functions of the c.m.s. energy \sqrt{s} . The full line is for $Re[d_\gamma]$. The dashed line is for $Im[d_\gamma]$. The dotted line is for $Re[d_Z]$. The dash-dotted line is for $Im[d_Z]$. In the figure we take $m_{h^0} = 100 \text{ GeV}$, $m_{H^0} = 200 \text{ GeV}$, $m_{H^\pm} = 150 \text{ GeV}$, $m_A = 250 \text{ GeV}$, $\alpha = \frac{\pi}{6}$, $\theta_1 = \frac{\pi}{4}$ and $\theta_2 = \frac{\pi}{2}$.

Fig.3(2) The electric and weak dipoles d_γ and d_Z as functions of the mass of h^0 . The full line is for $Re[d_\gamma]$. The dashed line is for $Im[d_\gamma]$. The dotted line is for $Re[d_Z]$. The dash-dotted line is for $Im[d_Z]$. In the figure we take $\sqrt{s} = 500 \text{ GeV}$, $m_{H^0} = 200 \text{ GeV}$, $m_{H^\pm} = 150 \text{ GeV}$, $m_A = 250 \text{ GeV}$, $\alpha = \frac{\pi}{6}$, $\theta_1 = \frac{\pi}{4}$ and $\theta_2 = \frac{\pi}{2}$.

Fig.3(3) The electric and weak dipoles d_γ and d_Z as functions of the mass of H^\pm . The full line is for $Re[d_\gamma]$. The dashed line is for $Im[d_\gamma]$. The dotted line is for $Re[d_Z]$. The dash-dotted line is for $Im[d_Z]$. In the figure we take $\sqrt{s} = 500 \text{ GeV}$, $m_{h^0} = 100 \text{ GeV}$, $m_{H^0} = 200 \text{ GeV}$, $m_A = 250 \text{ GeV}$, $\alpha = \frac{\pi}{6}$, $\theta_1 = \frac{\pi}{4}$ and $\theta_2 = \frac{\pi}{2}$.

Fig.3(4) The electric and weak dipoles d_γ and d_Z as functions of the mass of A^0 . The full line is for $Re[d_\gamma]$. The dashed line is for $Im[d_\gamma]$. The dotted

line is for $Re[d_Z]$. The dash-dotted line is for $Im[d_Z]$. In the figure we take $\sqrt{s} = 500 \text{ GeV}$, $m_{h^0} = 100 \text{ GeV}$, $m_{H^0} = 200 \text{ GeV}$, $m_{H^\pm} = 150 \text{ GeV}$, $\alpha = \frac{\pi}{6}$, $\theta_1 = \frac{\pi}{4}$ and $\theta_2 = \frac{\pi}{2}$.

Fig.3(5) The electric and weak dipoles d_γ and d_Z as functions of the phase angle θ_1 . The full line is for $Re[d_\gamma]$. The dashed line is for $Im[d_\gamma]$. The dotted line is for $Re[d_Z]$. The dash-dotted line is for $Im[d_Z]$. In the figure we take $\sqrt{s} = 500 \text{ GeV}$, $m_{h^0} = 100 \text{ GeV}$, $m_{H^0} = 200 \text{ GeV}$, $m_{H^\pm} = 150 \text{ GeV}$, $m_A = 250 \text{ GeV}$, $\alpha = \frac{\pi}{6}$ and $\theta_2 = 0$.

Fig.3(6) The electric and weak dipoles d_γ and d_Z as functions of the phase angle θ_2 . The full line is for $Re[d_\gamma]$. The dashed line is for $Im[d_\gamma]$. The dotted line is for $Re[d_Z]$. The dash-dotted line is for $Im[d_Z]$. In the figure we take $\sqrt{s} = 500 \text{ GeV}$, $m_{h^0} = 100 \text{ GeV}$, $m_{H^0} = 200 \text{ GeV}$, $m_{H^\pm} = 150 \text{ GeV}$, $m_A = 250 \text{ GeV}$, $\alpha = \frac{\pi}{6}$ and $\theta_1 = 0$.

Fig.4(1) The lepton charge distribution asymmetry A_{ch} and the forward-backward asymmetry A_{FB} as functions of the c.m.s. energy \sqrt{s} for the charged lepton (the product of the sequence decays $t \rightarrow b+W$ and $W \rightarrow l+\nu$). The full line is for $A_{ch} \times 10$. The dashed line is for A_{FB} . In the figure we take $m_{h^0} = 100 \text{ GeV}$, $m_{H^0} = 200 \text{ GeV}$, $m_{H^\pm} = 150 \text{ GeV}$, $m_A = 250 \text{ GeV}$, $\alpha = \frac{\pi}{6}$, $\theta_1 = \frac{\pi}{4}$, $\theta_2 = \frac{\pi}{2}$, and $\theta_0 = 30^\circ$.

Fig.4(2) The forward-backward asymmetry A_{FB} as a function of the masses of Higgs bosons h^0 , H^0 and H^\pm . The full line is for m_{h^0} with $m_{H^\pm} = 150 \text{ GeV}$ and $m_A = 250 \text{ GeV}$. The dashed line is for m_{H^0} with $m_{h^0} = 100 \text{ GeV}$ and $m_A = 250 \text{ GeV}$. The dotted line is for m_{A^0} with $m_{h^0} = 100 \text{ GeV}$ and $m_{H^\pm} = 150 \text{ GeV}$. In the figure we take $\sqrt{s} = 500 \text{ GeV}$, $m_H^0 = 200 \text{ GeV}$, $\alpha = \frac{\pi}{6}$, $\theta_1 = \frac{\pi}{4}$, $\theta_2 = \frac{\pi}{2}$, and $\theta_0 = 30^\circ$.

Fig.4(3) The lepton charge asymmetry A_{ch} as a function of the masses of Higgs bosons h^0 , H^0 and H^\pm . The full line is for m_{h^0} with $m_H^\pm = 150 \text{ GeV}$ and $m_A = 250 \text{ GeV}$. The dashed line is for m_{H^0} with $m_{h^0} = 100 \text{ GeV}$ and $m_A = 250 \text{ GeV}$. The dotted line is for m_{A^0} with $m_{h^0} = 100 \text{ GeV}$ and $m_{H^\pm} = 150 \text{ GeV}$. In the figure we take $\sqrt{s} = 500 \text{ GeV}$, $m_H^0 = 200 \text{ GeV}$, $\alpha = \frac{\pi}{6}$, $\theta_1 = \frac{\pi}{4}$, $\theta_2 = \frac{\pi}{2}$, and $\theta_0 = 30^\circ$.

Fig.4(4) The lepton charge distribution asymmetry A_{ch} and the forward-backward asymmetry A_{FB} as functions of the phase angle θ_1 . The full line

is for $A_{ch} \times 10$. The dashed line is for A_{FB} . In the figure we take $m_{h^0} = 100 \text{ GeV}$, $m_{H^0} = 200 \text{ GeV}$, $m_{H^\pm} = 150 \text{ GeV}$, $m_A = 250 \text{ GeV}$, $\alpha = \frac{\pi}{6}$, $\theta_1 = \frac{\pi}{4}$, $\theta_2 = \frac{\pi}{2}$ and $\theta_0 = 30^\circ$.

Fig.4(5) The lepton charge distribution asymmetry A_{ch} and the forward-backward asymmetry A_{FB} as functions of the phase angle θ_2 . The full line is for $A_{ch} \times 10$. The dashed line is for A_{FB} . In the figure we take $m_{h^0} = 100 \text{ GeV}$, $m_{H^0} = 200 \text{ GeV}$, $m_{H^\pm} = 150 \text{ GeV}$, $m_A = 250 \text{ GeV}$, $\alpha = \frac{\pi}{6}$, $\theta_1 = \frac{\pi}{4}$, $\theta_2 = \frac{\pi}{2}$ and $\theta_0 = 30^\circ$.

Fig.5(1) The average value of the spin-momentum correlation parameter ξ_{CP} as a function of the c.m.s. energy \sqrt{s} . In the figure we take $m_{h^0} = 100 \text{ GeV}$, $m_{H^0} = 200 \text{ GeV}$, $m_{H^\pm} = 150 \text{ GeV}$, $m_A = 250 \text{ GeV}$, $\alpha = \frac{\pi}{6}$, $\theta_1 = \frac{\pi}{4}$, $\theta_2 = \frac{\pi}{2}$, and $\theta_{cut} = 9^\circ$.

Fig.5(2) The average value of the spin-momentum correlation parameter ξ_{CP} as a function of the masses of Higgs bosons. The full line is for m_{h^0} with $m_{H^\pm} = 150 \text{ GeV}$ and $m_A = 250 \text{ GeV}$. The dashed line is for m_{H^\pm} with $m_{h^0} = 100 \text{ GeV}$ and $m_A = 250 \text{ GeV}$. The dotted line is for m_A with $m_{h^0} = 100 \text{ GeV}$ and $m_{H^\pm} = 150 \text{ GeV}$. In the figure we take $m_H^0 = 200 \text{ GeV}$, $\alpha = \frac{\pi}{6}$, $\theta_1 = \frac{\pi}{4}$, $\theta_2 = \frac{\pi}{2}$ and $\theta_{cut} = 9^\circ$.

Fig.5(3) The average value of the spin-momentum correlation parameter ξ_{CP} as function of the phase angles θ_1 and θ_2 . The full line is for θ_1 with $\theta_2 = 0$. The dashed line is for θ_2 with $\theta_1 = 0$. In the figure we take $\sqrt{s} = 500 \text{ GeV}$, $m_{h^0} = 100 \text{ GeV}$, $m_{H^0} = 200 \text{ GeV}$, $m_{H^\pm} = 150 \text{ GeV}$, $m_A = 250 \text{ GeV}$, $\alpha = \frac{\pi}{6}$ and $\theta_{cut} = 9^\circ$.

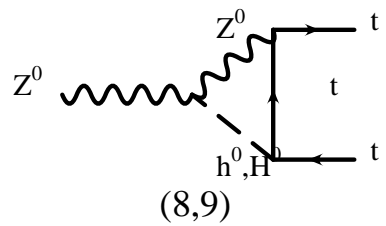
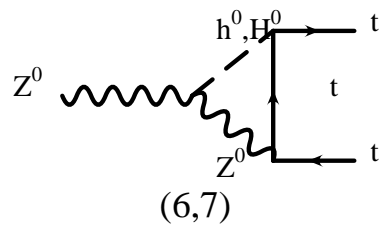
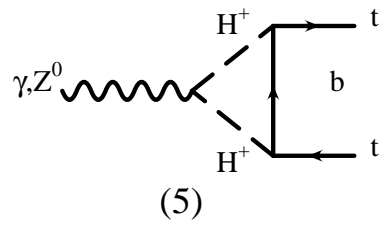
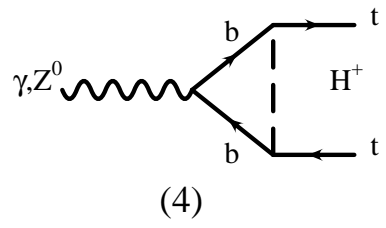
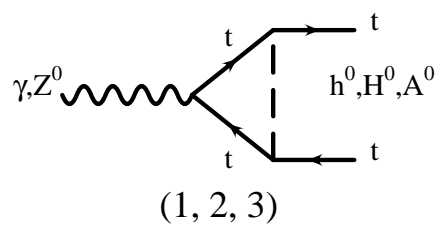


Fig.1

Fig.3(1)

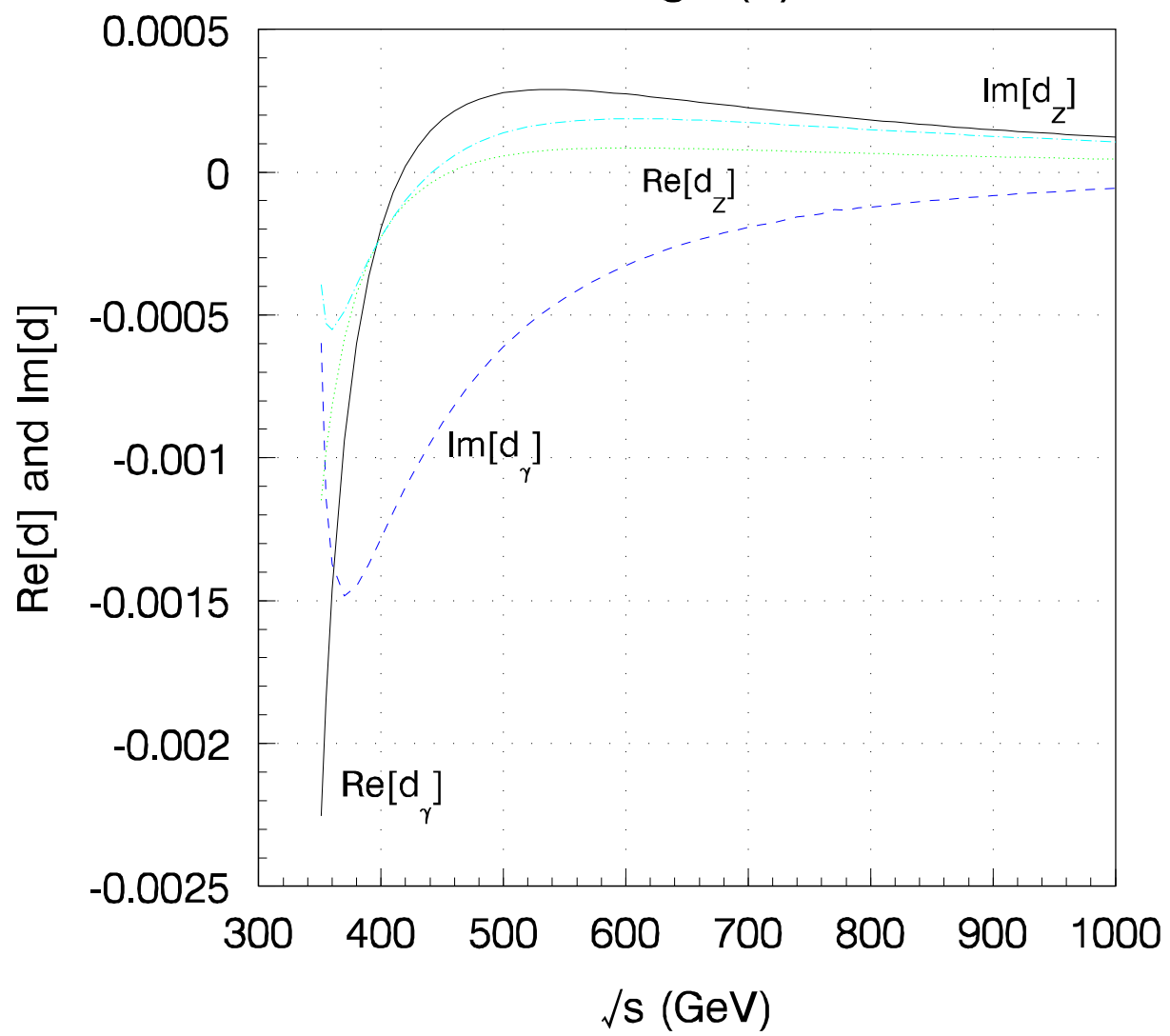


Fig.4(1)

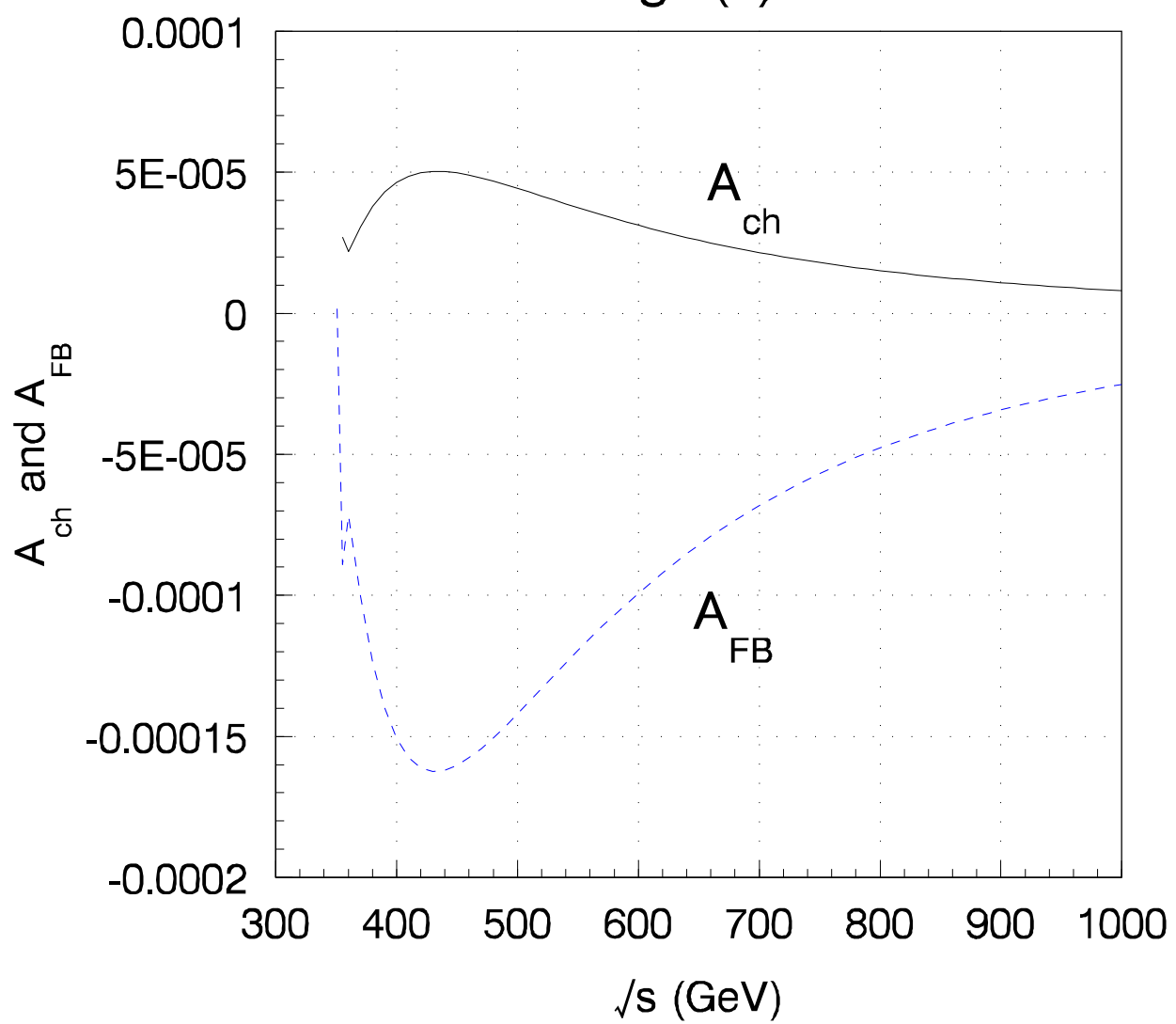
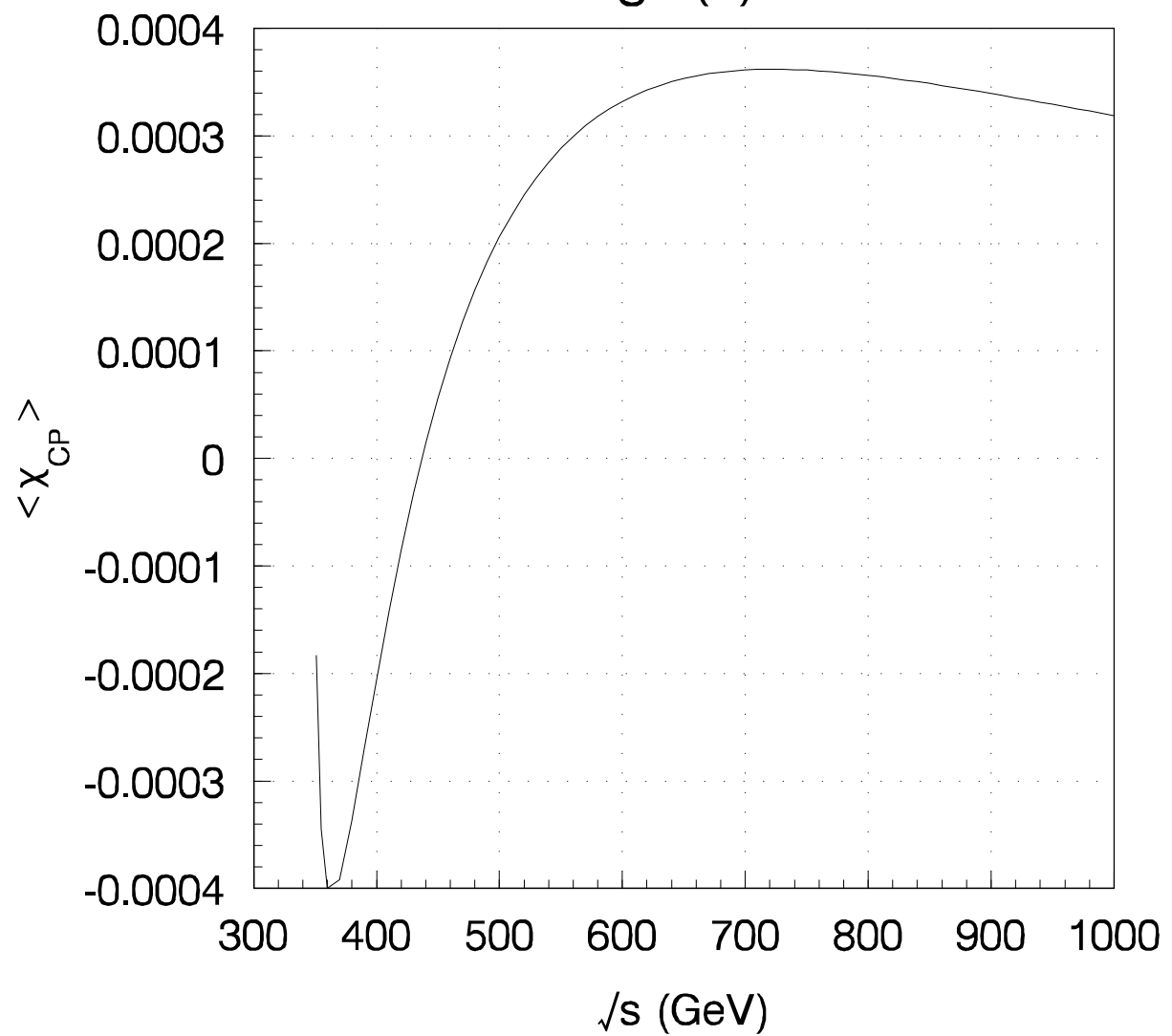


Fig.5(1)



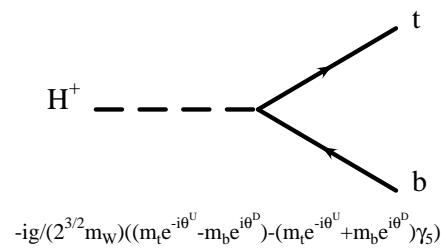
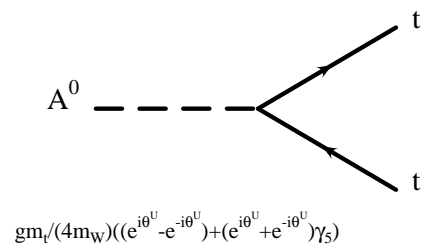
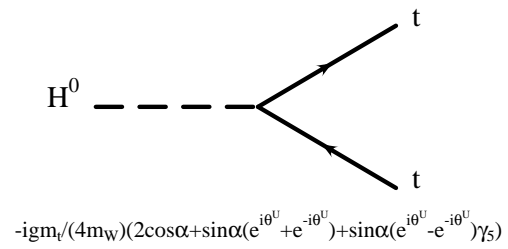
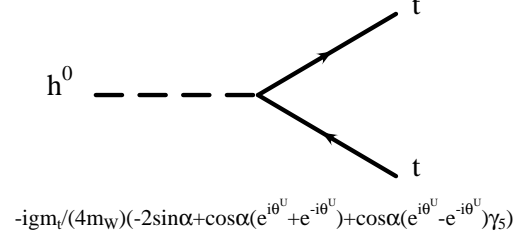


Fig.2

Fig.3(2)

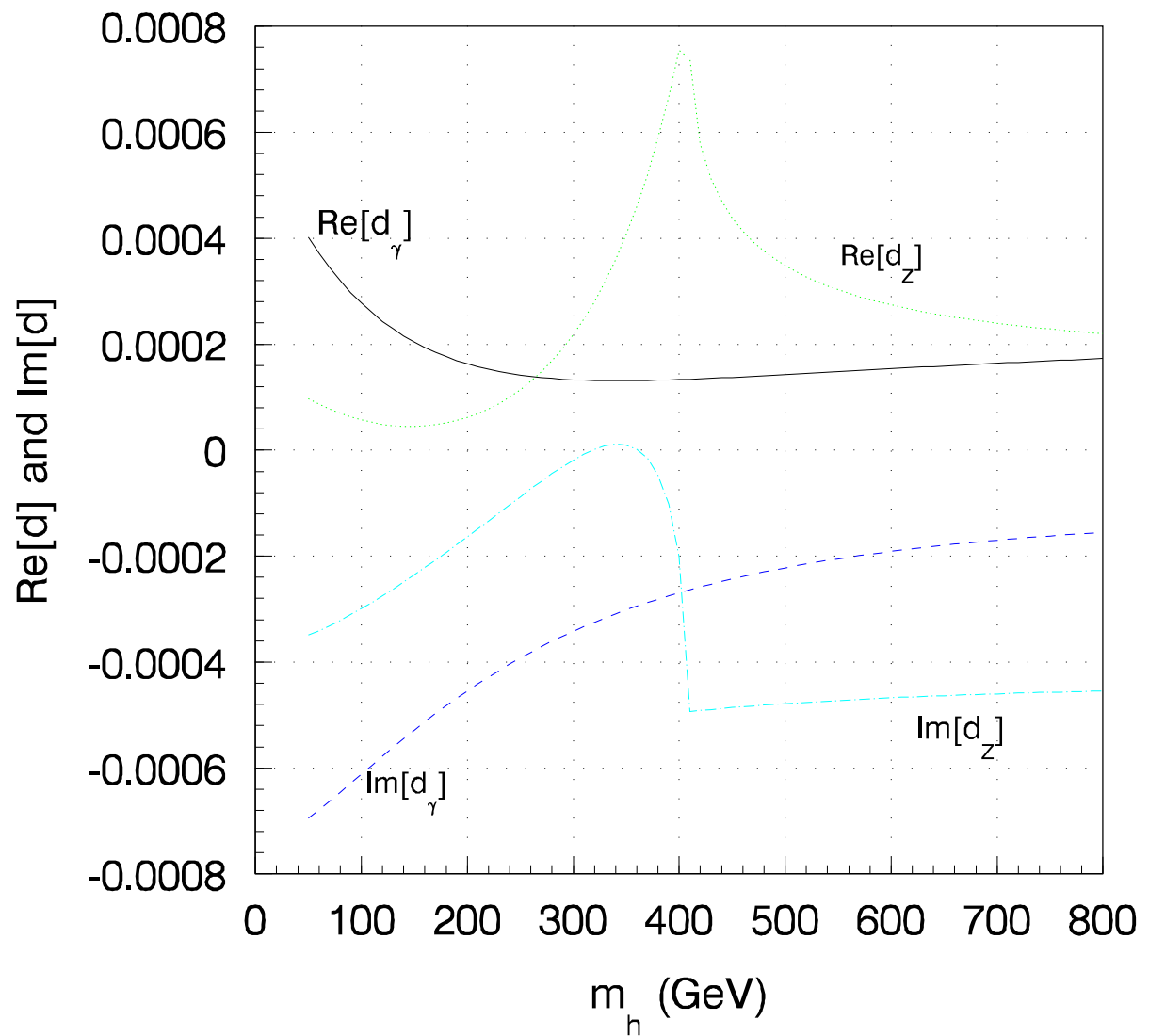


Fig.4(2)

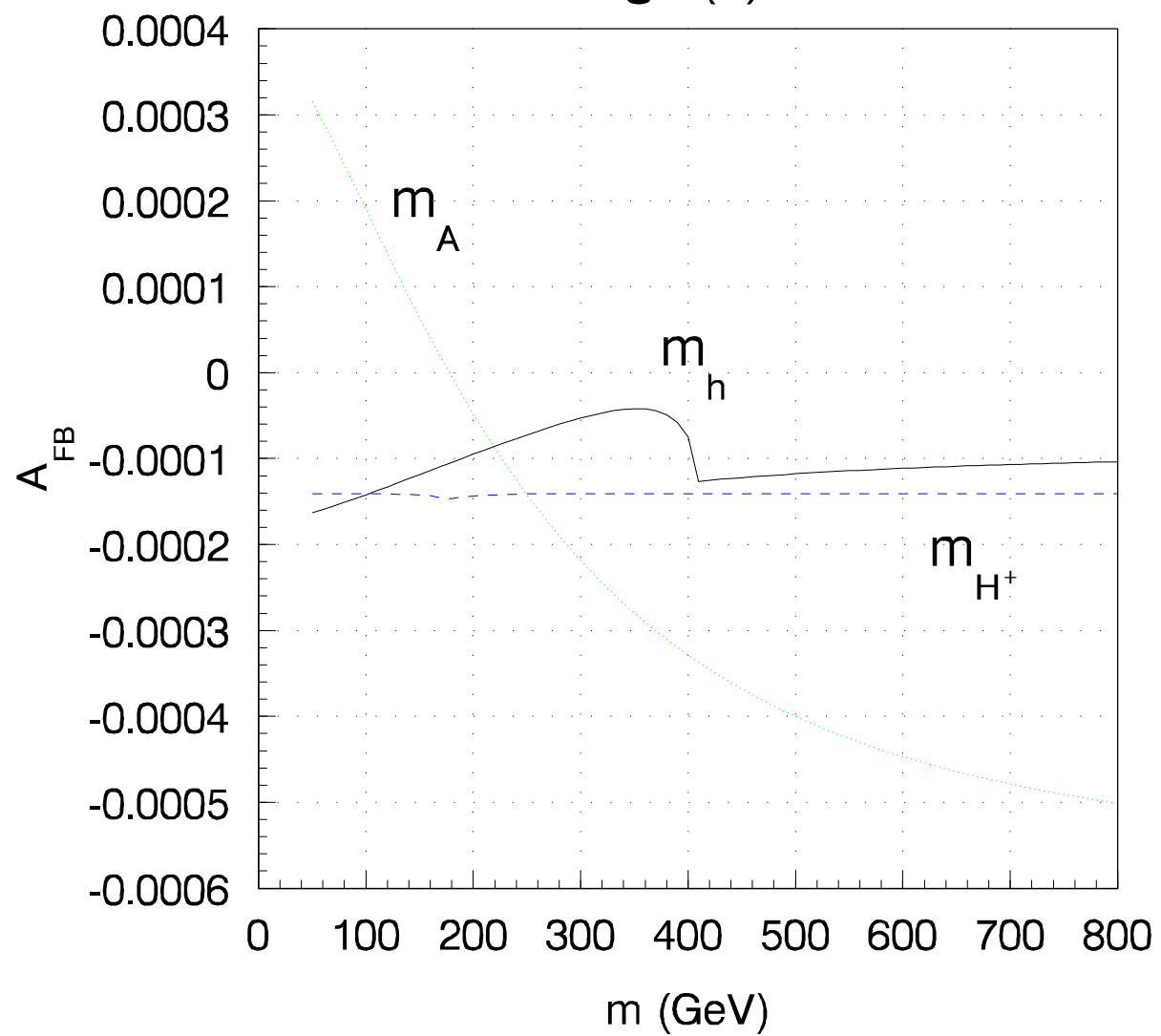


Fig.5(2)

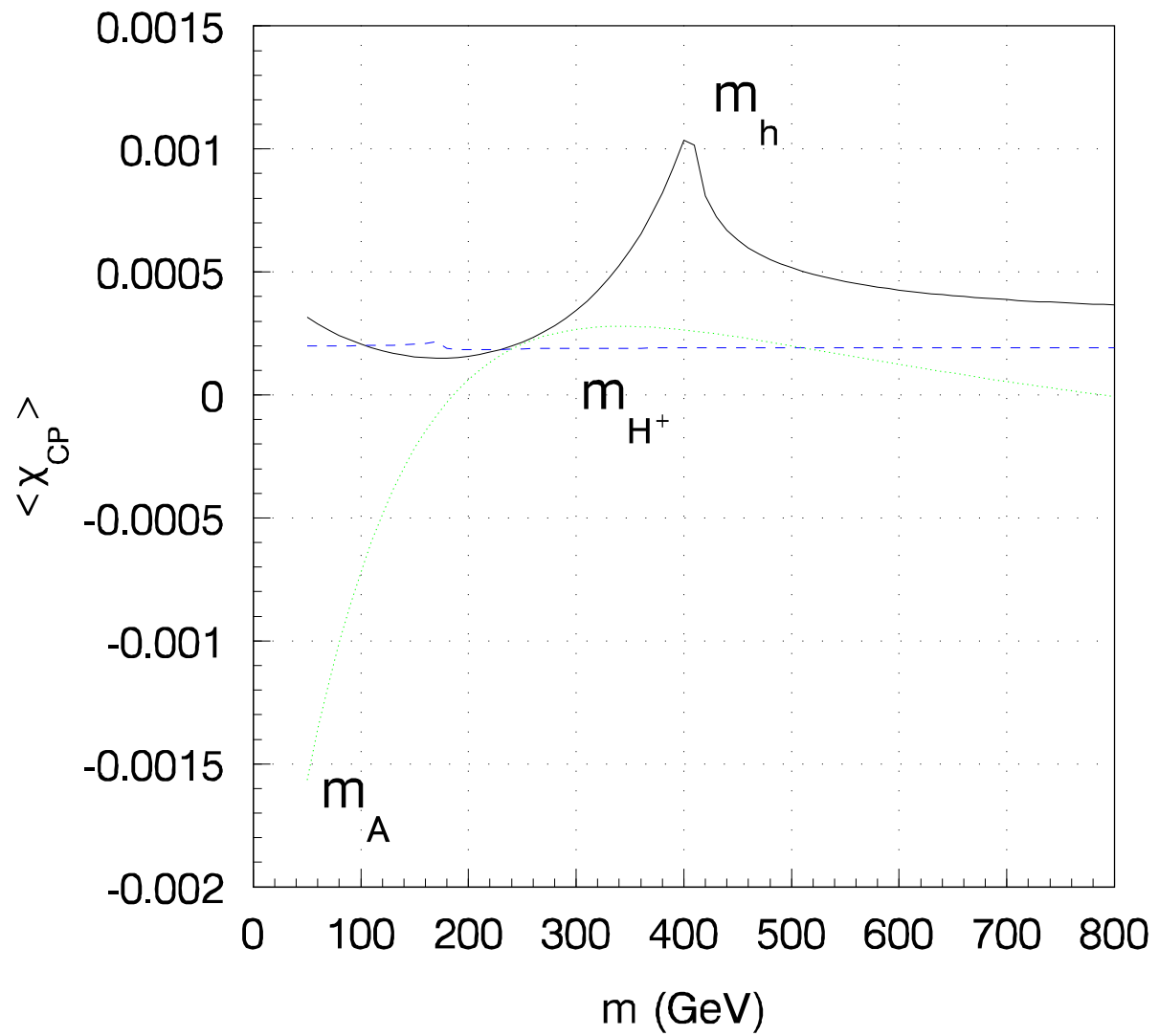


Fig.3(3)

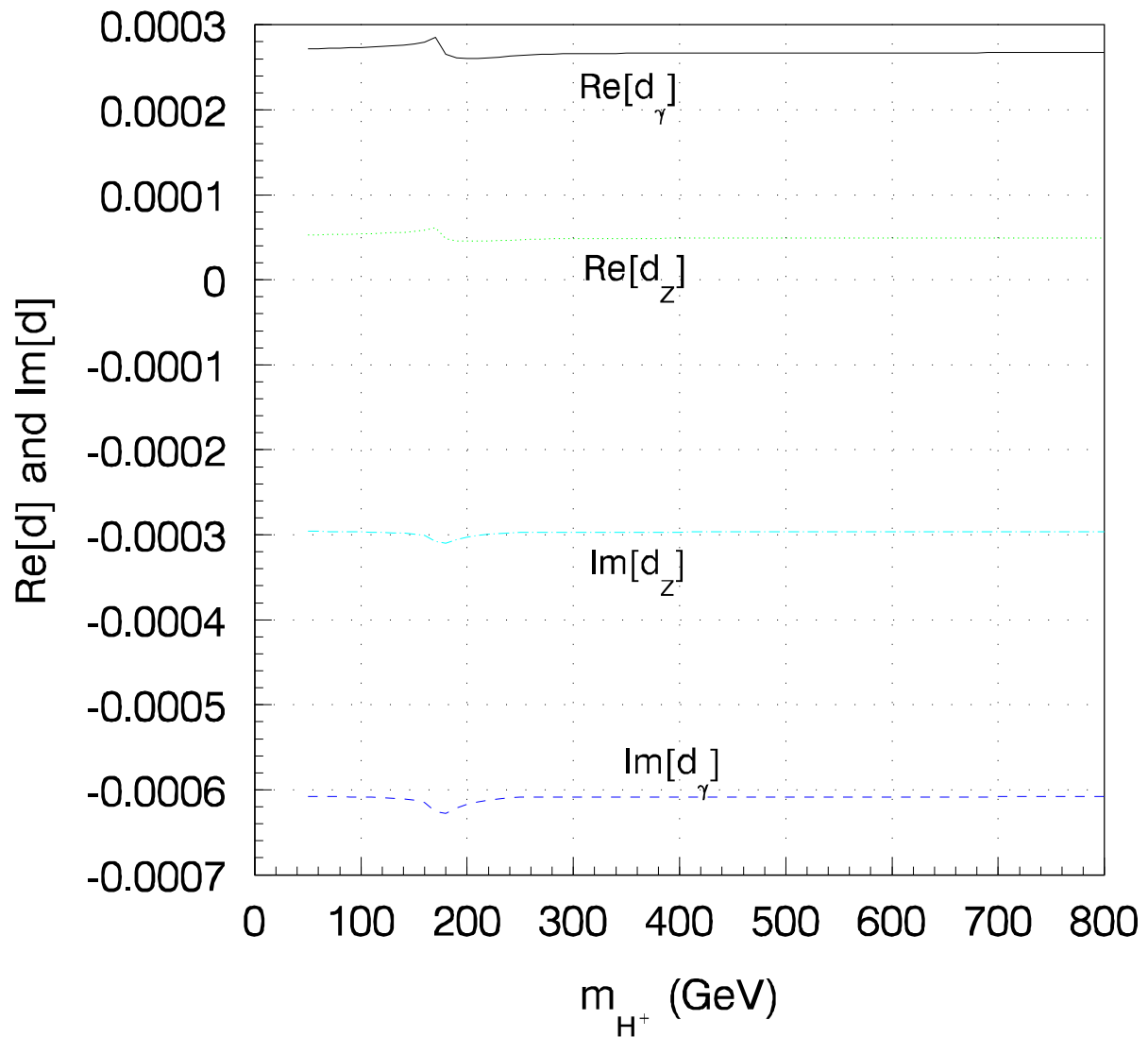


Fig.4(3)

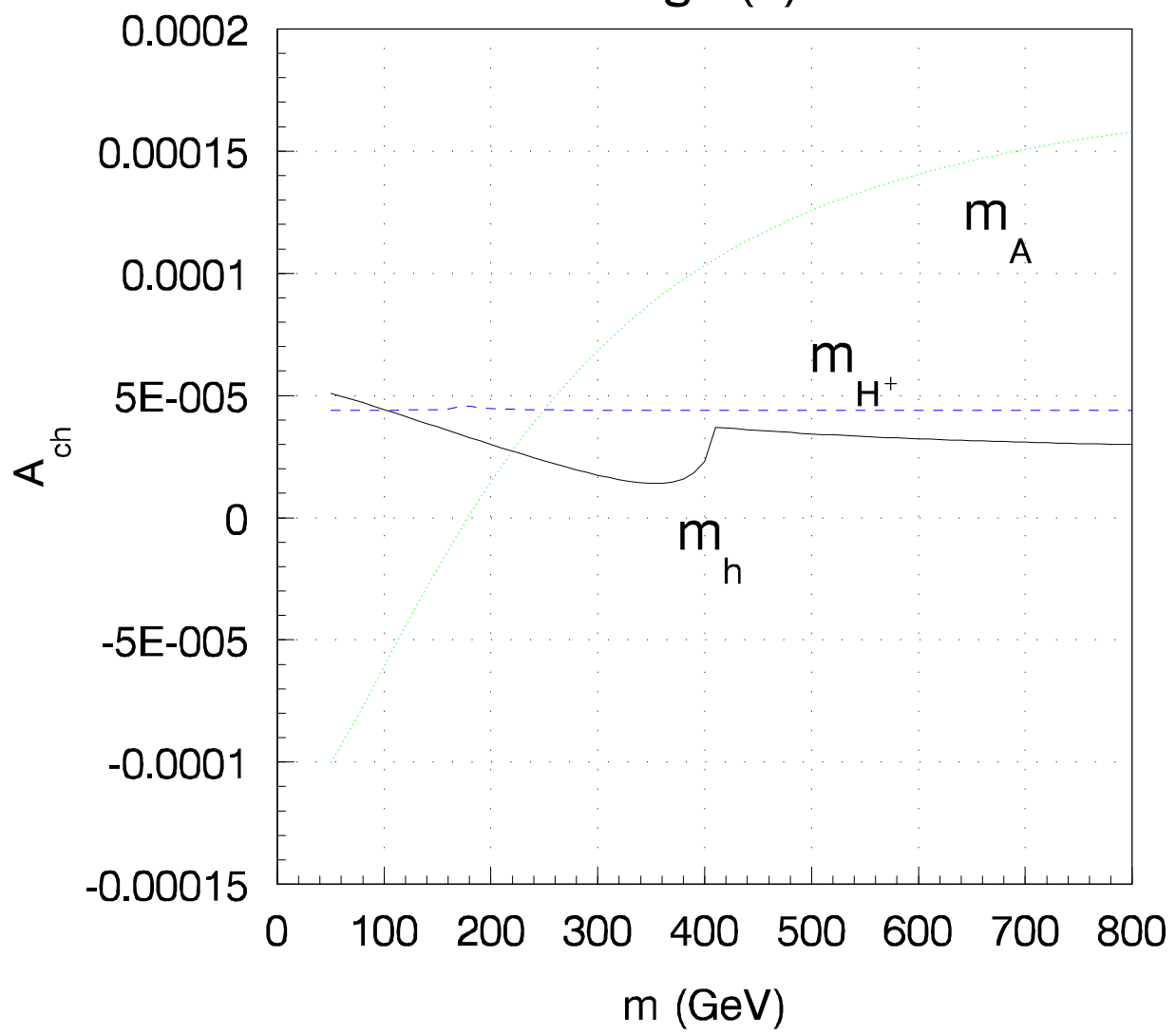


Fig.5(3)

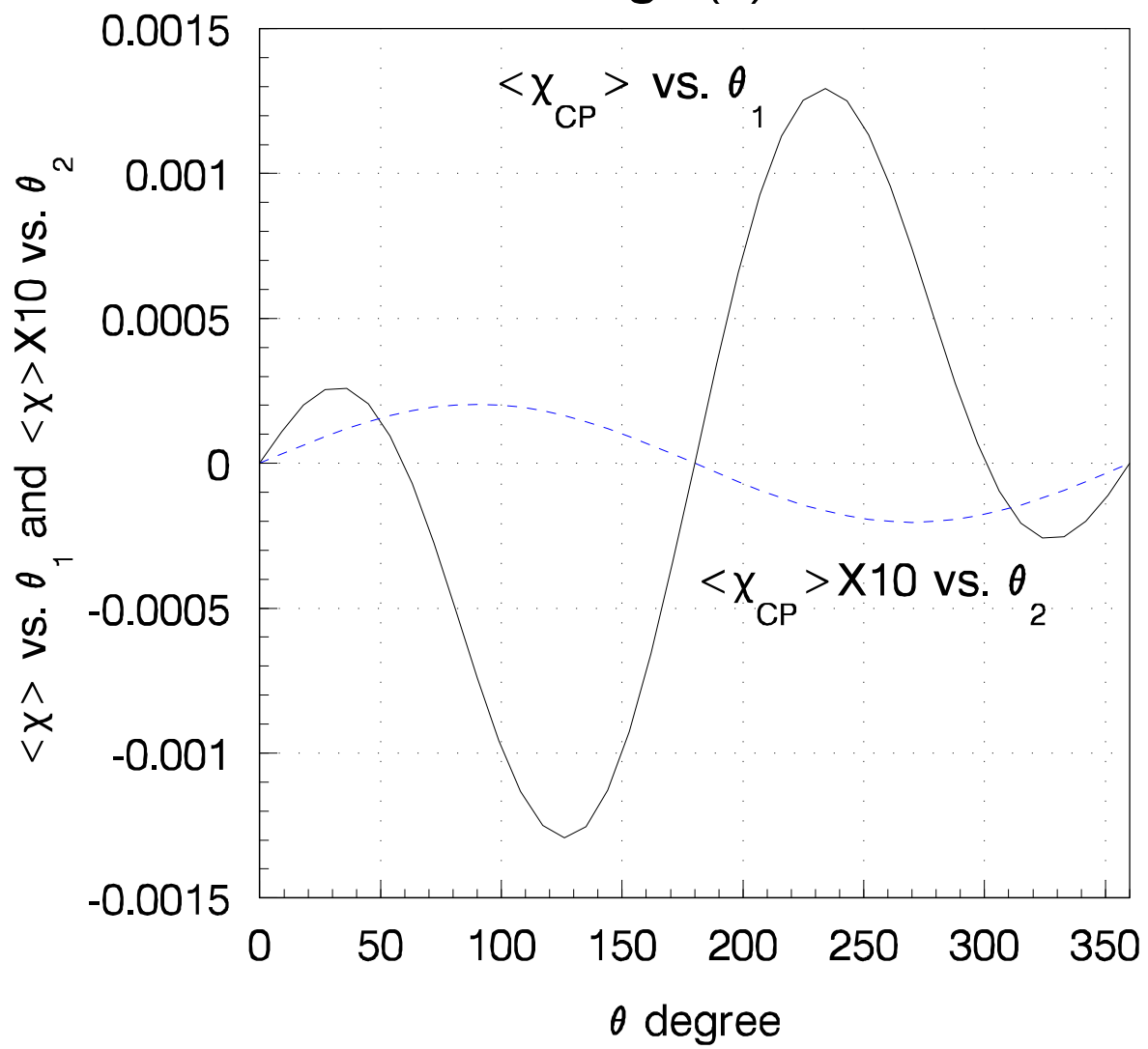


Fig.3(4)

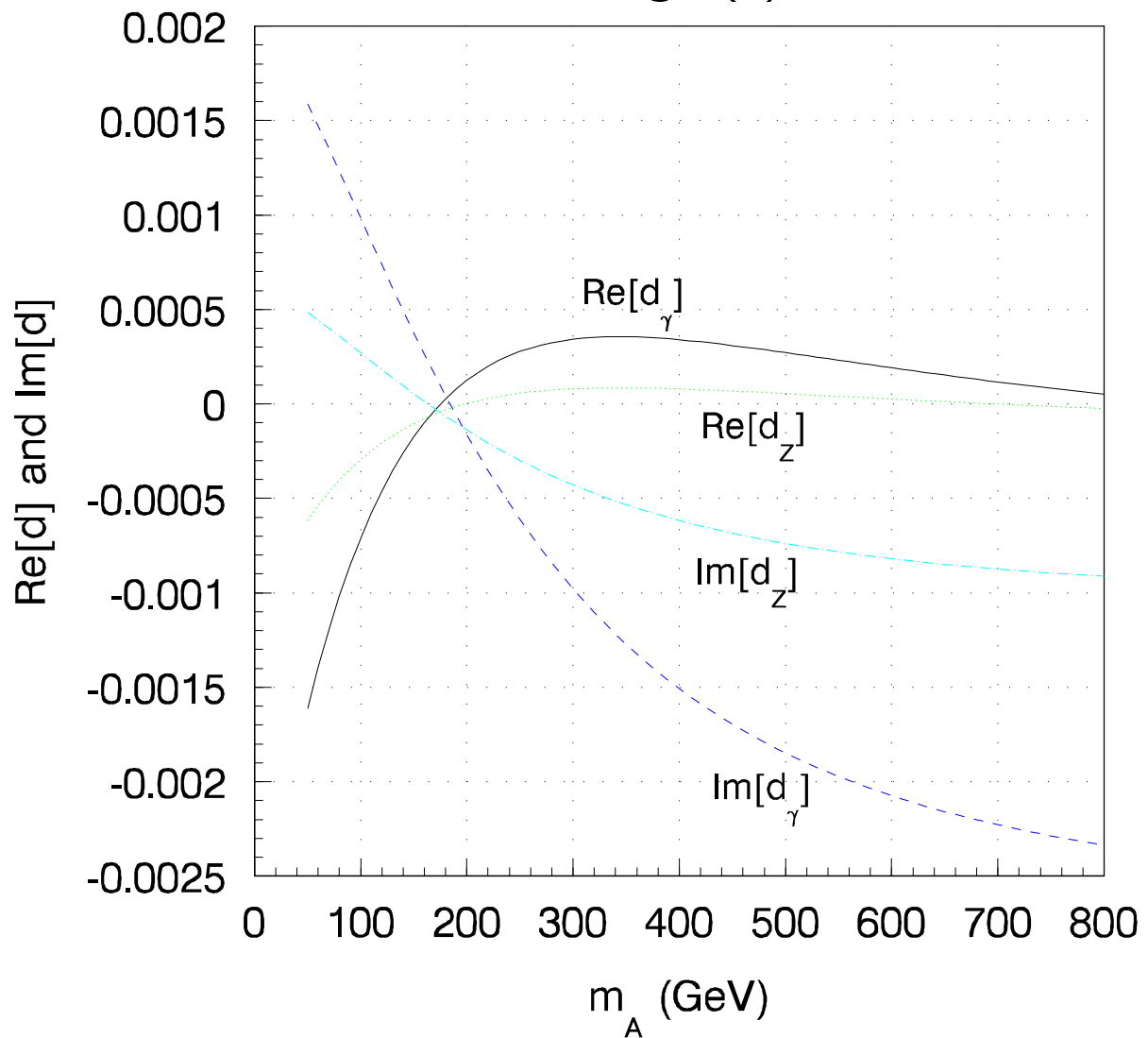


Fig.4(4)

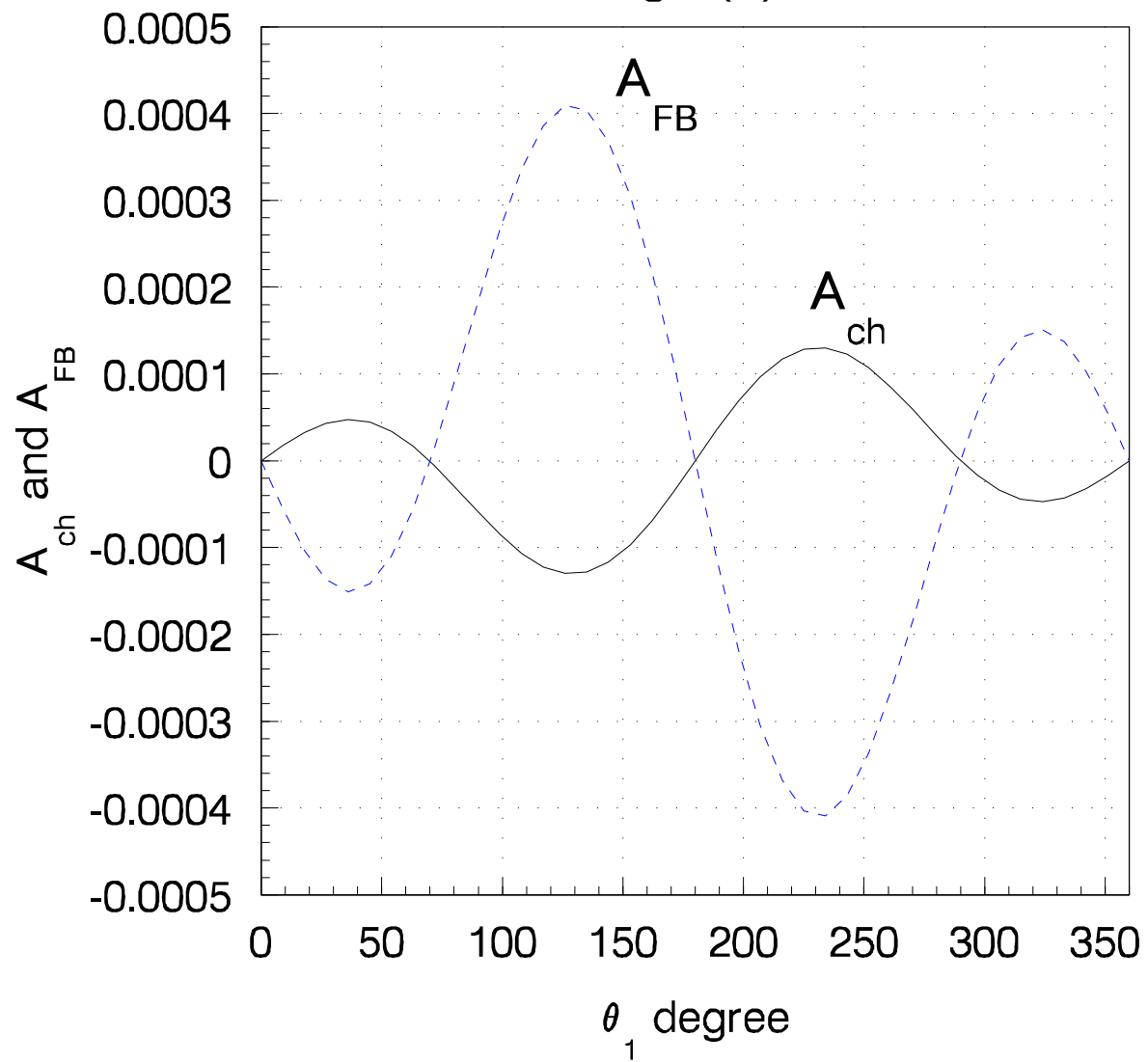


Fig.3(5)

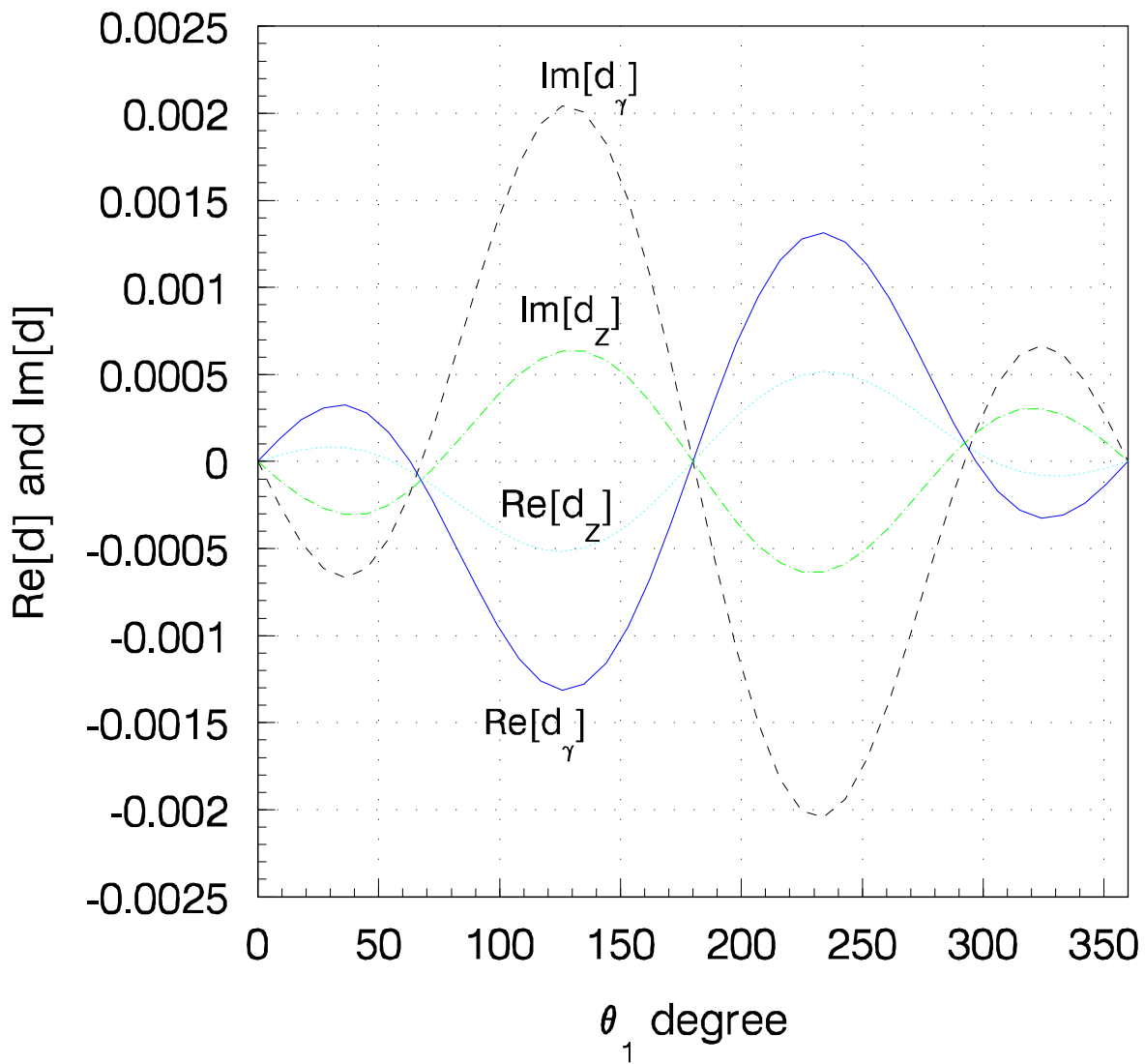


Fig.4(5)

